

A Hardware Neuronal Network Model of a Two-level Central Pattern Generator

Yoshinobu MAEDA*

Abstract This paper addresses hardware designs of a half-centered locomotor central pattern generator (CPG), composed of units reproducing the electrical behavior of neurons and synapses, such as action potentials, bursting discharges, and post-synaptic potentials. The typical phenomenon generated by the CPG is an alternating rhythmic activity of extensor and flexor sites, in the absence of external rhythmic input. In order to reproduce the deletion phenomena, or the phase resetting and non-resetting rhythmic activities observed after during spontaneous cessation of activity, a two-level CPG network and unit burst generators (UBGs) were proposed by Rybak et al. (2006) from the viewpoint of mathematical modeling. The deletion at the first level, i.e., the rhythm generator (RG) level, caused the post-deletion rhythm to be phase shifted (reset) with respect to the pre-deletion rhythm. However, the deletion at the second level, i.e., the pattern formation (PF) level, caused the post-deletion rhythm to be un-phase shifted (non-reset) with respect to the pre-deletion rhythm. This paper confirms that such deletion phenomena, or the phase resetting and non-resetting phenomena, could be well reproduced in the hardware design of a two-level CPG using the electronic circuit simulator SPICE. In particular, it has been clarified that non-resetting deletions appeared, even with the cessation of activity occurring at any phase with respect to the observed temporal bursting. Hardware synapse models, phenomenologically reproducing excitatory and inhibitory post-synaptic potentials (EPSP and IPSP), were newly designed in order to connect the hardware neuron models, proposed by Hoshimiya et al. (1979) for the excitable and/or oscillatory neuron, and by Maeda and Makino (2000) for the bursting neuron.

Keywords: bursting neuron, excitatory and inhibitory synapses, deletion, phase shift, Darlington

connection.

Received

* Niigata University

1. Introduction

A typical neuronal membrane possesses an ability to generate electrical activity when the input stimulation is beyond the threshold. An action potential, or a firing, is itself an activity and is regarded as biological information unit, e.g., the sequential action potentials cause muscle contraction. Many mathematical models, described by differential equations, have been developed to investigate the mechanism of neuronal activity. Hardware modeling is also one method to clarify the mechanism. This is advantageous from the following three standpoints: 1) it is a high speed processor, 2) the energy consumption necessary to process neuronal information can be evaluated [1], and 3) it is easy to apply to industrial technology such as robotics [2-3]. In the third case, not only neuron models must be developed, but also synapse models are required to connect the hardware neurons. However, modeling using commercial electronic devices, limiting the electrical dynamics to the regulated behavior, is not easy. In this paper, a hardware design of both excitatory and inhibitory synapses, composed of minimal electronic devices, is proposed and the temporal dynamics similar to the post-synaptic potential have been reproduced phenomenologically. The main purpose of this study is, furthermore, to design a central pattern generator (CPG) using the hardware neurons and synapses designed, and to reproduce the deletion phenomena [4-5] occurred with spontaneous cessations of activity.

CPG [4-7] is known as a physiological operation in animals that can produce the basic locomotor rhythm in the absence of any rhythmic input from the higher brain and peripheral sensory feedback. However, the physiological mechanism of CPG, based on the neuronal organization, is unknown. The first conceptual scheme was developed based on a half-center concept. In this concept, one half-center excites synergistic motoneurons and activates interneurons, inhibiting antagonist motoneurons. This primary concept cannot explain the deletion phenomena, especially non-resetting deletions, after the cessation of activity. Rybak et al. [4-5] explains completely the deletion phenomena in terms of Hodgkin-Huxley [8] type of mathematical CPG models, composed of two-level half-centers; one level

being named the rhythm generator neurons, and the other, the pattern formation neurons. The author proposed a hardware design, comprising a two-level CPG to reproduce the deletion phenomena. Here, the author assumed that the deletions result from additional excitatory and inhibitory drive that changes the excitability of particular neurons, similar to the plausible assumption of Rybak et al. [4].

2. Hardware neurons

Neuronal membranes are classified into two types: one is the excitable and/or oscillatory membrane, which generates an action potential when the membrane potential exceeds the threshold, and the other is the bursting membrane, which generates sequential action potentials (active phase) between relatively long quiescent states (silent phase). Hoshimiya et al. [9] constructed a hardware model of the excitable/oscillatory membrane composed of a few electrical devices, i.e., three bi-polar transistors, three resistors and two conductors, as shown in Fig. 1. C_m and R_m represent the membrane capacitance and leakage resistance, respectively. The membrane potential, V_m , and the refractory equivalent potential, V_r [10], are measured at C_m and C_1 , respectively. Similarly to the Hodgkin-Huxley model [8], the resting potential and the outside of the membrane is assumed to be 0V (ground). When external current input raises V_m to exceed the threshold regulated by the voltage 0.8V of between base and emitter of the bipolar transistor, Tr_1 , the transient inward current (upward arrow in Fig. 1) flows instantaneously from the constant voltage source, E , into C_m via bipolar transistor, Tr_2 , so that the depolarizing phase in an action potential is observed. This current also flows into C_1 , whose voltage, V_r , is proportional to the integral of the current with respect to time. When V_r exceeds threshold regulated by the base-emitter voltage of the bipolar transistor, Tr_3 , the delayed outward current (downward arrow in Fig. 1) flows from C_m to the ground via Tr_3 , so that the repolarizing phase in an action potential is observed.

A bursting neuron model, alternating the active and silent phases, theoretically requires at least one other equivalent potential [11-14], and, as such, requires three capacitances in the minimal hardware

Fig. 1
←

design [15-16]. Maeda and Makino [15] proposed a hardware model of the bursting membrane by means of dividing the two-terminal circuit branch responsible for delayed outward current into two, in parallel with the other branches (Fig. 2). One circuit branch generates the fast outward current (thick solid arrow in Fig. 2), responsible for the refractoriness of an action potential beyond the threshold of the base-emitter voltage of Tr_1 . The base-emitter connection of Tr_4 contributes to the membrane potential to maintain it over the threshold, and as a result, the action potential can continuously be observed as the active phase of bursting. The other branch generates a slow outward current (thick dotted arrow in Fig. 2) responsible for generating the silent phase of bursting, i.e., it pulls down the membrane potential below the threshold. To reproduce the slowness and prolong the active phase of bursting, the values of R_2 and C_2 were set greater than those of $R_1 = 20 \text{ k}\Omega$ and $C_1 = 1 \text{ }\mu\text{F}$. In this paper, values of $C_2 = 10 \times C_1 = 10 \text{ }\mu\text{F}$ and $R_2 = 15 \times R_1 = 300 \text{ k}\Omega$ were adopted, and, as a result, the time constant, described by R_2C_2 , of the slow equivalent potential, V_s , measured at C_2 was 150 times greater than that of the fast equivalent potential, V_r , measured at C_1 , i.e., $R_2C_2 = 150 \times R_1C_1$.

Fig. 2



Typical temporal waveforms of the membrane potential of hardware excitable/oscillatory and bursting neuron models are shown in Fig. 3 (a) and (b), respectively, using the electronic circuit simulator SPICE with a step of 0.5 ms. In these cases, neuron models are driven by an externally injected constant current of 0.1mA.

Fig. 3



3. Hardware synapses

Synapses are functionally classified into two types, i.e., gap junctions and chemical synapses. In the gap junction, a current, proportional to the voltage, flows interactive between neurons, so that the device resistor is used to develop such bi-direction currents [1]. On the other hand, a chemical synapse limits neuronal communication to be unidirectional, from pre-synaptic to post-synaptic cells. In addition, it shows transient behavior of post-synaptic current, only when a pre-synaptic cell is firing [17]. Therefore,

a hardware design of the chemical synapse is not as simple as the gap junction. However, the hardware model focused on synaptic plasticity [18] is so complicated that it is not suitable for the CPG network, as shown in the next section. For this work, it was necessary for the synapse model to be satisfied with just three conditions as follows:

- 1) Synaptic behavior does not influence the pre-synaptic site,
- 2) A synapse functions only when the pre-synaptic site is firing, and
- 3) Temporal summation of the post-synaptic potentials is reproduced in the post-synaptic site.

Fig. 4



Figure 4 (a) shows the excitatory synapse model, presented using a simple and minimal design, which generates an approximated excitatory post-synaptic potential (EPSP). This reproduces the most common non-NMDA synapse that physiologically uses the neurotransmitter glutamate, and is described by a time-dependent synaptic conductance, $1/R_{out}$, and a synaptic battery, E_{syn} , relevant to a reversal potential. Such a synapse isolates the electrical properties of the post-synaptic site from the pre-synaptic one. To this end, the synapse model is wired up between neurons via a high input resistance, R_{in} , ($= 9.1 \text{ M}\Omega$) and a low output resistance, R_{out} , (variable according to the situation). The input resistance, in this case, is set relatively large, so that very little current flows through it. Therefore, the pre-synaptic cell does not change its own state because it has difficulty in supplying current to the following synapse (Condition 1). A serial connection, or so-called Darlington connection, of Tr_1 and Tr_2 regulates the collector-emitter current of Tr_3 . When the membrane potential of the pre-synaptic model is greater than two base-emitter voltages (Tr_1 and Tr_2), i.e., when the membrane potential of pre-synaptic model has already been firing (Fig. 4 (c)-(1)), the base current of Tr_3 , induced by the base-emitter current of Tr_1 and Tr_2 , flows (Fig. 4 (c)-(2) and (3)). The collector-emitter current of Tr_3 , induced by the base current, then flows from E_{syn} to the membrane capacitance of post-synaptic model via the output resistance R_{out} (Fig. 4 (c)-(4)). This collector-emitter current of Tr_3 constitutes the depolarizing phase of EPSP while the pre-synaptic model is firing. Without a base current flowing in Tr_3 , mediated by the membrane potential

of pre-synaptic model becoming lower than the two base-emitter voltages of Tr_1 and Tr_2 of the synapse, the collector-emitter current from E_{syn} stops flowing (Fig. 4 (c)-(5), (6) and (7)) and the repolarizing phase of EPSP begins (Condition 2). The membrane leakage resistance of the post-synaptic model, in parallel with the charged membrane capacitance, plays an important role in the repolarizing phase of EPSP, i.e., the membrane capacitance is discharged through the membrane leakage resistance.

Similarly, the design of the inhibitory synapse is shown in Fig. 4(b). In this case, E_{syn} is in the opposite direction, and, as such, extracts the current from post-synaptic model to the synapse model when the pre-synaptic model is firing. Accompanying this change of direction, the emitter and collector of Tr_3 are interchanged in the inhibitory synapse model. This opposite flow of the current generates an inhibitory post-synaptic potential (IPSP) so as to hyperpolarize the post-synaptic potential.

Suppose that these synapse models, connected with post-synaptic simple model composed of only C_m and R_m , are driven by pre-synaptic pulse voltages (amplitude 5V, width 3ms), as shown in Figs. 5(a) and 5(b). Then, typical temporal waveforms of both excitatory and inhibitory post-synaptic potentials (EPSP and IPSP) are shown in Fig. 5(c), using the electronic circuit simulator SPICE with a step of 0.5 ms. In the circuit in Fig. 5(a), the current flows from E_{syn} to C_m via R_{out} during pulses, and, thus, charges C_m positively. Without pulses, the current flows from C_m to the ground via R_m , discharging C_m . As a result, one EPSP is observed. In the circuit in Fig. 5(b), one IPSP is observed by means of the reversal of the current flows. These potentials in the post-synaptic sites, EPSP and IPSP, can be integrated so as to memorize temporal information of pre-synaptic firings (condition 3). Thus the post-synaptic model, whose input comprises the synapse model, is able to reproduce phenomenologically, EPSP, IPSP and their temporal summation, in terms of a leaky-integration (Fig.5 (c)).

Fig. 5



4. Hardware two-level CPG

This section presents the design of the CPG network proposed by Rybak et al. [4] using the hardware

bursting model, hardware excitable/oscillatory model, hardware excitatory and inhibitory synapse models, in Fig. 6. The inside of one hardware model, depicted by top of Fig. 1 and 2, was connected to the inside of the others through the synapse models. In the Rybak model, the rhythm generator (RG), pattern formation (PF) and interneurons (IN) are composed of multiple networks, based on the Hodgkin-Huxley type conductance-based neuron model. The hardware network shown in Fig. 6 replaces such massive neurons by a single hardware model. One may interpret that single hardware model is a model of massive neurons, and, as such, generates the synchronized dynamics of the collective firing of every neuron. In the Rybak model, furthermore, the RG and the PF are composed of UBGs, whereas the interneuron models comprise excitatory/inhibitory ones. In the hardware case proposed in this paper, the only RG employed was the bursting model [15], whereas the PF and the IN were designed with excitable/oscillatory model [9]. Bursting neurons, in general, are regarded as being available for drawing target neurons into a synchronized rhythm [19]. The RG needs the bursting model in the sense that generates a basic rhythm, but the PF does not necessarily require. Therefore, in the hardware configuration, shown in Fig. 6, both the PF and the IN, were designed using excitatory/inhibitory models, for simplification.

Fig. 6



The RGs are weakly interactive ($R_{out} = 1M\Omega$) using the excitatory synapse (ES), because they are synchronized without inhibitory connections [4]. Simultaneously, the RGs activate the interneuron INRGs (via $R_{out} = 51k\Omega$) inhibiting antagonist RGs and PFs (via $R_{out} = 100k\Omega$). The PFs are also received weakly from agonist RGs via the excitatory synapse ($R_{out} = 500k\Omega$), and activate the interneuron INPFs inhibiting antagonist PF (via $R_{out} = 51k\Omega$). The RGs and PFs are driven by the midbrain locomotor regions (MLR), which are hypothesized as constant voltage stimulations in this model, via $51k\Omega$ resistances.

Fig. 7



Typical temporal waveforms of the RGs, the INRGs, the PFs, and the INPFs are shown in Fig. 7 using the electronic circuit simulator SPICE with a step of 0.5 ms. In order to set different initial

conditions of the extensor from those of the flexor, the external injected constant voltages are set with a subtle difference between them ($V_{MLR}^{(X)}=1.01V$ (X: RG-E or PF-E), and $1.0V$ (X: RG-F or PF-F)). Alternative bursting phenomena were then observed between the extensor and flexor sites because of the influence of inhibitory synaptic connections.

To observe the spontaneous errors in the rhythmic activity of motoneurons occurring during fictive locomotion and scratch, or so-called appearance of deletion phenomena, V_{MLR} was temporarily changed, as similarly noted by Rybak et al. [4], and as shown in Fig. 8 (using SPICE with a step of 0.5 ms). In Fig. 8 (a), the activity of RG-E was additionally driven by a MLR of 10V from 13 to 15 seconds, seen as the top trace in Fig. 8 (a). This produced sustained activity in the RG-E and substantially reduced opposing activity (RG-F). This phenomenon was also successful to the PF level. A few firings observed in the PF level were caused by the silent phase of bursting in the RG level. What is important to note is that the onset and offset of the temporary change in RG excitability occur at an arbitrary time with respect to the locomotor rhythm. Therefore, resetting deletions (phase shift), noted by Rybak et al. [4], would be observed in the firing regenerated after a two-second perturbation. In fact, when the first spike of bursting is assumed to be the phase zero, the phase shifts, ϕ_i , were observed in the post-deletion rhythm. In this example, all phases were delayed, i.e., every phase shift, ϕ_i , was positive. In Fig. 8 (b), the activity of RG-F was additionally inhibited by an MLR of 0.1V from 13 to 15 seconds, seen in the top trace in Fig. 8 (b). Similarly, the resetting deletions were observed in the firing, regenerated after the two-second perturbation. During the perturbation to RG-F, the activities of the flexor sites were reduced, and only the activity of PF-E was increased, as might have been expected. The perturbation inhibited caused the transitional firing to be temporarily prolonged at the post-deletion rhythm in the flexor sites (from 15 to 16 seconds, shown in Fig. 8 (b)).

In Fig. 8 (c), the activity of PF-E was additionally driven by an MLR of 5V from 13 to 15 seconds, seen in the top trace in Fig. 8 (c). This produced sustained activity in the PF-E and substantially reduced

Fig. 8



activity in opposition (PF-F), whereas the activity of RGs did not change, because the network architecture indicated no relation between the activity of RGs and the stimulation to PFs. In this case, the non-resetting deletions (no phase shift), noted by Rybak et al. [4], were observed in the firing regenerated after a two-second perturbation, i.e., the rhythms of the PFs were swiftly synchronized to those of the RGs, irrespective of the perturbation. The perturbation to the PF did not reset the locomotor rhythm, as Rybak and his coworkers observed in their numerical simulations. In Fig. 8 (d), the activity of PF-F was additionally inhibited by the MLR of 0.5V from 13 to 15 seconds, seen in the top trace in Fig. 8 (d). Similarly, non-resetting deletion phenomena were observed in the firing regenerated after the two-second perturbation. During perturbation to the PF-F, the activity of the PF-F was reduced, whereas the activity of PF-E was hardly changed. In summary, the hardware design presented here could reproduce the same dynamics as the numerical simulations of Hodgkin-Huxley type mathematical models.

Fig. 9

In order to quantitatively evaluate the amount of the phase shift, the onset of a two-second additional stimulation was changed, and the phase shifts, ϕ_i , observed from 15 to 24 seconds were measured. Example cases of RG-E and PF-F are illustrated in Fig. 9 (a) and (b), respectively. The perturbation timing, t , or the onset, depicted in horizontal axes, is normalized by the period of bursting $T \doteq 0.64$ sec, and the average phase shifts, ϕ , are plotted on the vertical axes. The temporal waveforms of one period, corresponding to the normalized phase, are drawn below. In Fig. 9 (a), the averages of the phase shift, ϕ , increased with t . The tendency of the regression equation of ϕ on t was evaluated as 0.75. Therefore, the additional stimulation into RG-E caused the resetting deletion, except for $t \doteq 0.3$, i.e., after 0.192 sec ($t \times T$) from the beginning of bursting. Roughly, the perturbation in the active phase of bursting caused the phase to be advanced, and the perturbation in the silent phase of bursting caused the phase to be delayed. On the other hand, in Fig. 9 (b), the averages of the phase shift, ϕ , were almost constant around zero vs t . The tendency of the regression equation of ϕ on t was evaluated as 0.03, or almost equal to



zero. Therefore, any timing (onset) of additional stimulation to the PF resulted in non-resetting deletion.

5. Conclusion

This paper has presented a two-level central pattern generator (CPG), composed of bursting and excitatory/oscillatory hardware units, or neuron models [9,15], and excitatory and inhibitory hardware connectors, or synapse models. This two-level CPG architecture in the hardware design reproduced a so-called deletion phenomena, i.e., resetting and non-resetting of the phase were observed in the post-deletion rhythm, as mathematically or numerically explained by Rybak et al. [4]. Additional stimulation into the rhythm generator (RG) level generally caused the deletion reset. In particular, in the active phase of bursting, the phase advanced, whilst in the silent phase, the phase was delayed. On the other hand, it has been clarified that non-resetting deletions appeared, even with the cessation of activity occurring at any phase with respect to the observed temporal bursting of the pattern formation (PF) level.

In order to construct the afferent feedback, it is necessary to model hardware motoneurons (output units) to connect with the CPG proposed in this paper. The future work is to construct a locomotion robot including the CPG, driven by the biological and physiological mechanisms. A requirement for the biological locomotion robot is that the control should be based on the CPG, composed of neuron models reproducing the action potentials. The hardware models proposed in this paper satisfy the above requirement. It is possible, furthermore, that the relationship between the locomotion and the power consumption could be investigated, using such hardware locomotion machinery.

References

1. Y. Maeda, E. Yagi and H. Makino: Synchronization with low power consumption of hardware models of cardiac cells. *BioSystems*. 79, 125-131, 2005.
2. M. A. Lewis, R. Etienne-Cummings, A. H. Cohen and M. Hartmann: Toward biomorphic control

- using custom aVLSI CPG chips. Int. Conf. IEEE Robotics and Automation, 1, 494-500, 2000.
3. M. Nakanishi, T. Nomura and S. Sato: Stumbling with optimal phase reset during gait can prevent a humanoid from falling. Biol. Cybern. 95(5), 503-515, 2006.
 4. I. A. Rybak, N. A. Shevtsova, M. Lafreniere-Roula and D. A. McCrea: Modelling spinal circuitry involved in locomotor pattern generation: insights from deletions during fictive locomotion. J Physiol. 577(2), 617-639, 2006.
 5. I. A. Rybak, K. Stecina, N. A. Shevtsova and D. A. McCrea: Modelling spinal circuitry involved in locomotor pattern generation: insights from the effects of afferent stimulation. J Physiol. 577(2), 641-658, 2006.
 6. A. Frigon, G. Barriere, K. Fenelon and S. Yakovenko: Conceptualizing the mammalian locomotor central pattern generator with modeling. J. Physiol. 580, 363-364, 2007.
 7. D. A. McCrea and I. A. Rybak: Organization of mammalian locomotor rhythm and pattern generation. Brain Res. Reviews, 57, 134-146, 2008.
 8. A. L. Hodgkin and A. F. Huxley: A quantitative description of membrane current and its application to conduction and excitation in nerve. J Physiol. 117, 504-544, 1952.
 9. N. Hoshimiya, S. Yoshida, K. Shogen, T. Matsuo: Two-terminal electronic circuit neuron model with excitable membrane $V-I-t$ characteristics. Biol. Cybern. 35, 125-130, 1979.
 10. T. B. Kepler, L. F. Abbott and E. Marder: Reduction of conductance-based neuron models. Biol. Cybern. 66, 381-387, 1992.
 11. R. Bertram, M. J. Butte, T. Kiemel and A. Sherman: Topological and phenomenological classification of bursting oscillations. Bull. Math. Biol. 57, 413-439, 1995.
 12. F. C. Hoppensteadt and E. M. Izhikevich: Weakly connected neural networks. Springer, 1997.
 13. Y. Maeda, K. Pakdaman, T. Nomura, S. Doi and S. Sato: Reduction of a model for an *Onchidium* pacemaker neuron. Biol. Cybern. 78, 265-276, 1998.

14. M. I. Rabinovich, P. Varona, A. I. Selverston and H. D. I. Abarbanel: Dynamical principles in neuroscience. *Rev. Mod. Phys.* 78, 1213-1265, 2006.
15. Y. Maeda and H. Makino: A pulse-type hardware neuron model with beating, bursting excitation and plateau potential. *BioSystems*. 58, 93-100, 2000.
16. K. Saeki and Y. Sekine: CMOS implementation of neuron models for an artificial auditory neural network. *IEICE Trans. Fundamentals*. E86-A(2), 424-427, 2003.
17. C. Koch: *Biophysics of computation*. Oxford University Press, 1999.
18. Y. Hayashi, K. Saeki and Y. Sekine: A synaptic circuit of a pulse-type hardware neuron model with STDP. *International Congress Series*, 1301, pp.132-135, 2007.
19. H. Jahnsen and R. Llinas: Ionic basis for the electroresponsiveness and oscillatory properties of Guinea-Pig thalamic neurons *in vitro*. *J. Physiol.* 349, 227-247, 1984.

Yoshinobu MAEDA

Fig. 1 Hardware configuration of the excitable/oscillatory membrane proposed by Hoshimiya et al. [9]. The top and bottom of the circuit represent the inside and outside of the membrane, respectively. $E = 5$ V, $C_m = C_1 = 1 \mu\text{F}$, $R_m = R_0 = 100 \text{ k}\Omega$, $R_1 = 20 \text{ k}\Omega$.

Fig. 2 Hardware configuration of the bursting membrane proposed by Maeda and Makino [15]. The top and bottom of the circuit represent the inside and outside of the membrane, respectively. $E = 5$ V, $C_m = C_1 = 1 \mu\text{F}$, $C_2 = 10 \mu\text{F}$, $R_m = R_0 = 100 \text{ k}\Omega$, $R_1 = 20 \text{ k}\Omega$, $R_2 = 300 \text{ k}\Omega$.

Fig. 3 Typical temporal waveforms of the membrane potentials. (a) Hardware excitatory/oscillatory neuron model. (b) Hardware bursting neuron model. Externally injected constant current was 0.1 mA.

Fig.4 Hardware configuration of (a) excitatory and (b) inhibitory synapses. R_{in} and R_{out} are the input and output resistances, respectively. R_{in} is fixed at 9.1 M Ω and R_{out} is variable according to the situation.

(c) Qualitative operational mechanism of the onset of EPSP. (1) pre-synaptic cite fires (“L→H”), (2) base-emitter currents of Tr_1 and Tr_2 flow, (3) base current of Tr_3 follows, (4) collector-emitter current of Tr_3 flows and, simultaneously, the onset of EPSP appears, (5) base-emitter currents of Tr_1 and Tr_2 cease (depicted by the dashed arrows) when the pre-synaptic site becomes quiescent (“H→L”), (6) base current of Tr_3 also stops and, finally, (7) collector-emitter current of Tr_3 , responsible for the onset of EPSP, stops.

Fig. 5 (a) Excitatory synapse driven by a pre-synaptic pulse voltage and the post-synaptic simple R_m - C_m model (passive model). (b) Inhibitory synapse driven by a pre-synaptic pulse voltage and the post-synaptic simple R_m - C_m model (passive model). (c) Typical temporal waveforms of EPSP and IPSP ($R_{out} = 30 \text{ k}\Omega$). The dotted lines represent the voltage pulse stimulation of the input.

Yoshinobu MAEDA

Fig. 6 (a) Schematic diagram of the two-level CPG. (b) Hardware configuration of the two-level CPG.

“-E” and “-F” represent the extensor and flexor side, respectively. “RG”, “PF”, “IN”, “ES” and “IS” represent rhythm generator, pattern formation, interneuron, excitatory and inhibitory synapses, respectively. Only RG was composed from the bursting model. Black and white arrows represent the excitatory and inhibitory flows of electrical information, respectively. $V_{MLR}^{(RG-E)}$, $V_{MLR}^{(RG-F)}$, $V_{MLR}^{(PF-E)}$ and $V_{MLR}^{(PF-F)}$ are external inputs (MLR) of RG-E, RG-F, PF-E and PF-F, respectively.

Fig. 7 Typical temporal waveforms of the membrane potentials from the hardware CPG model.

Externally injected constant voltage is 1.01V in RG-E and PF-E, and 1.0V in RG-F and PF-F.

Fig. 8 Simulations of resetting deletions (phase shift) in (a) and (b), and non-resetting deletions (no phase shift) in (c) and (d) for the CPG model. RGs and PFs are originally driven by $V_{MLR}=1.01V$ and $=1V$, respectively. During 2 seconds from 13 to 15, the CPG model is additionally driven by the step-wise perturbation of (a) $V_{MLR}^{(RG-E)} = 10V$, (b) $V_{MLR}^{(RG-F)} = 0.1V$, (c) $V_{MLR}^{(PF-E)} = 5V$, and (d) $V_{MLR}^{(PF-F)} = 0.5V$.

Fig. 9 Simulations of (a) resetting and (b) non-resetting deletions. Average phase shift ϕ vs normalized phase of perturbation t . Normalized phase corresponds to the temporal waveforms illustrated below. The active phase of bursting corresponds to the duration from 0.0 to 0.4 of the normalized phase.

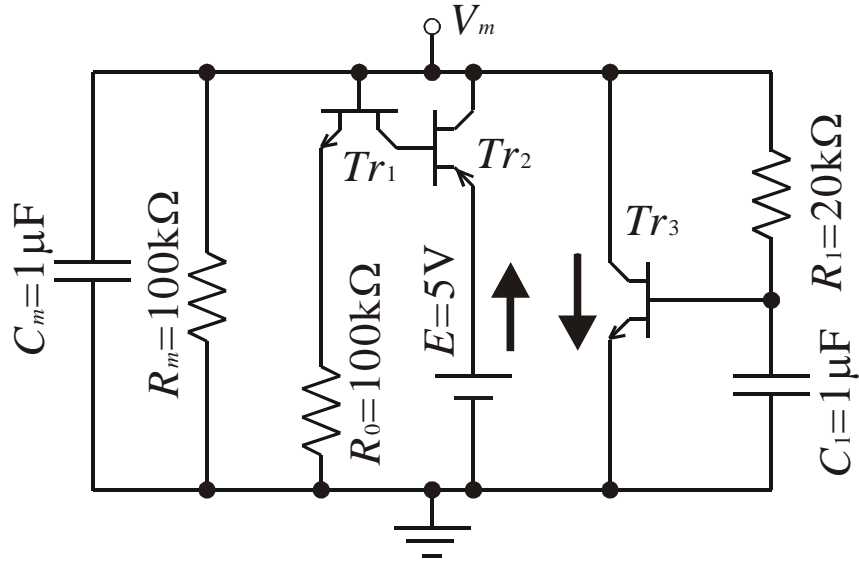


Fig. 1 Hardware configuration of the excitable/oscillatory membrane proposed by Hoshimiya et al. [9].

The top and bottom of the circuit represent the inside and outside of the membrane, respectively. $E = 5$

V, $C_m = C_1 = 1 \mu F$, $R_m = R_0 = 100 k\Omega$, $R_1 = 20 k\Omega$.

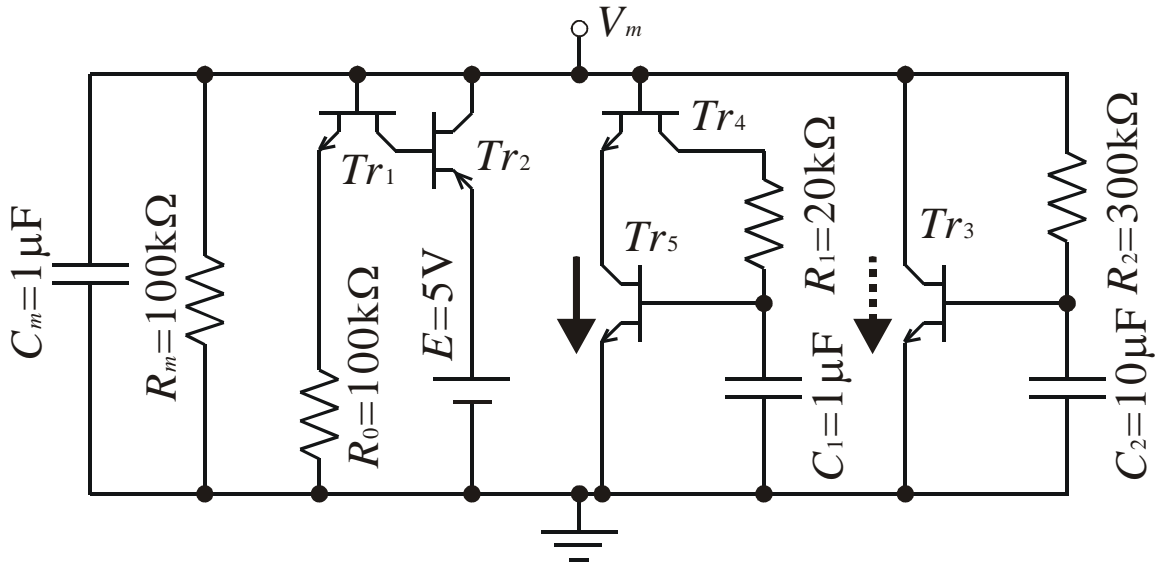


Fig. 2 Hardware configuration of the bursting membrane proposed by Maeda and Makino [15]. The top and bottom of the circuit represent the inside and outside of the membrane, respectively. $E = 5 \text{ V}$, $C_m = C_1 = 1 \text{ } \mu\text{F}$, $C_2 = 10 \text{ } \mu\text{F}$, $R_m = R_0 = 100 \text{ k}\Omega$, $R_1 = 20 \text{ k}\Omega$, $R_2 = 300 \text{ k}\Omega$.

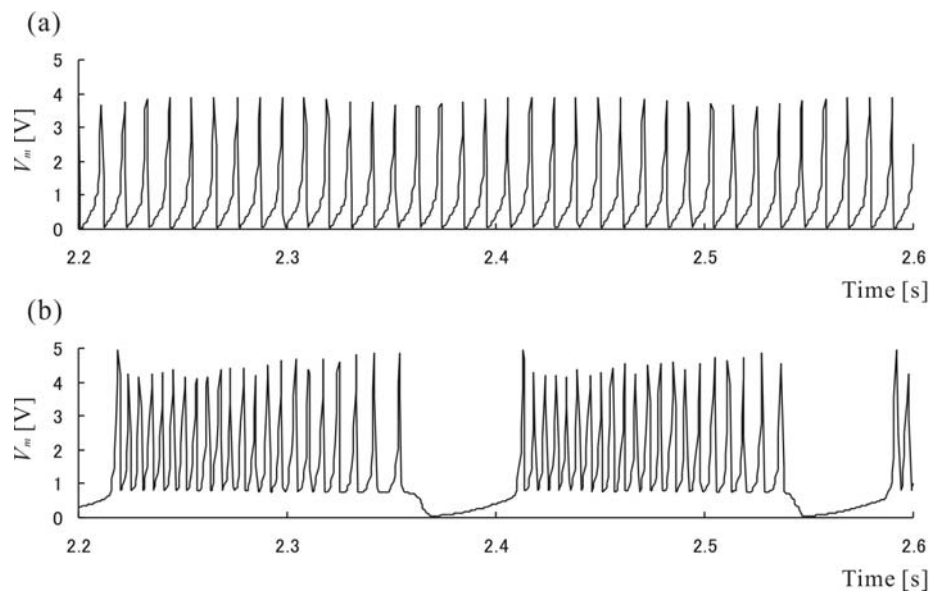


Fig. 3 Typical temporal waveforms of the membrane potentials. (a) Hardware excitatory/oscillatory neuron model. (b) Hardware bursting neuron model. Externally injected constant current was 0.1mA.

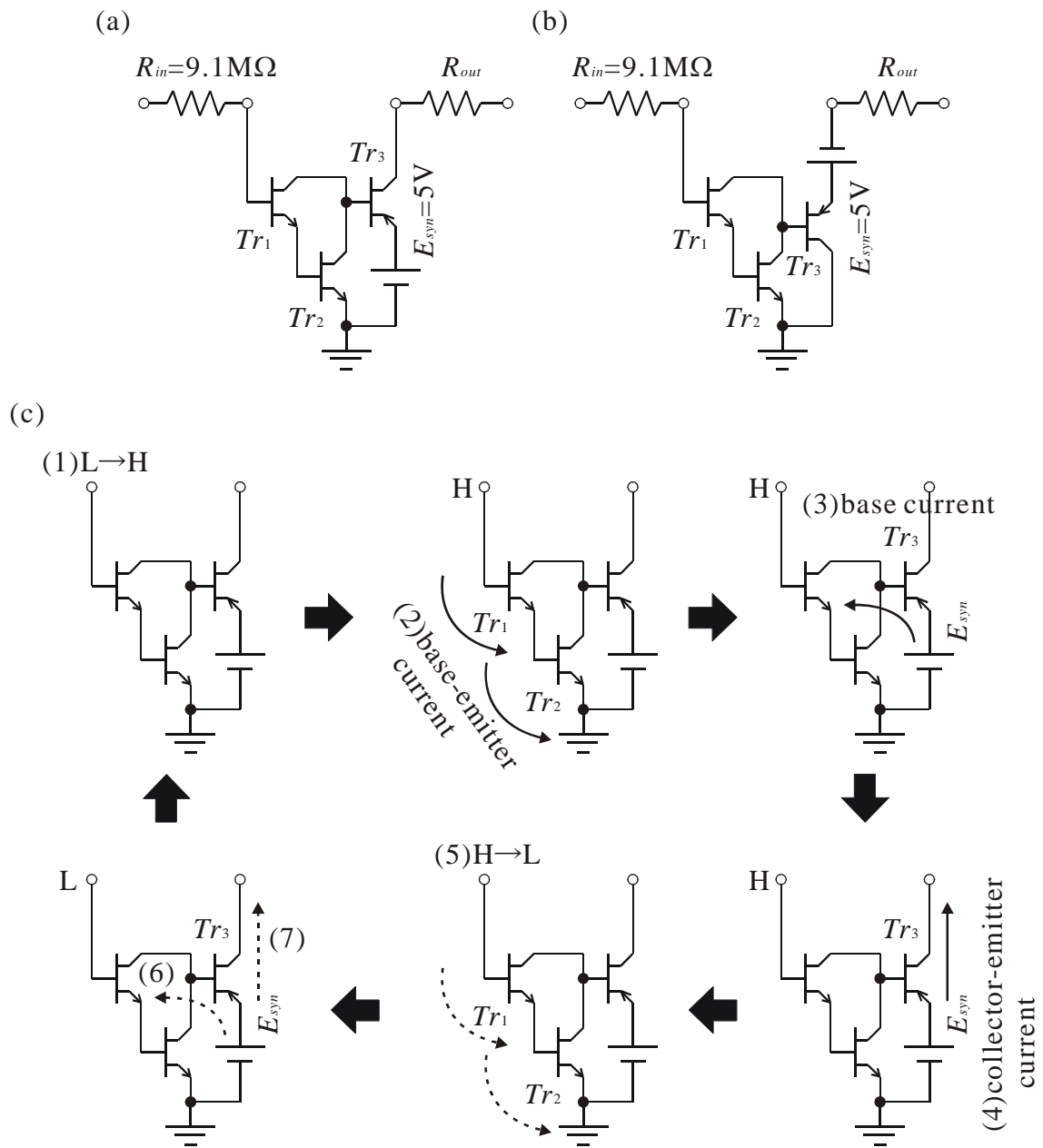


Fig. 4 Hardware configuration of (a) excitatory and (b) inhibitory synapses. R_{in} and R_{out} are the input and output resistances, respectively. R_{in} is fixed at $9.1\text{M}\Omega$ and R_{out} is variable according to the situation. (c) Qualitative operational mechanism of the onset of EPSP. (1) pre-synaptic cite fires (“L→H”), (2) base-emitter currents of Tr_1 and Tr_2 flow, (3) base current of Tr_3 follows, (4) collector-emitter current of Tr_3 flows and, simultaneously, the onset of EPSP appears, (5) base-emitter currents of Tr_1 and Tr_2 cease (depicted by the dashed arrows) when the pre-synaptic site becomes quiescent (“H→L”), (6) base current of Tr_3 also stops and, finally, (7) collector-emitter current of Tr_3 , responsible for the onset of EPSP, stops.

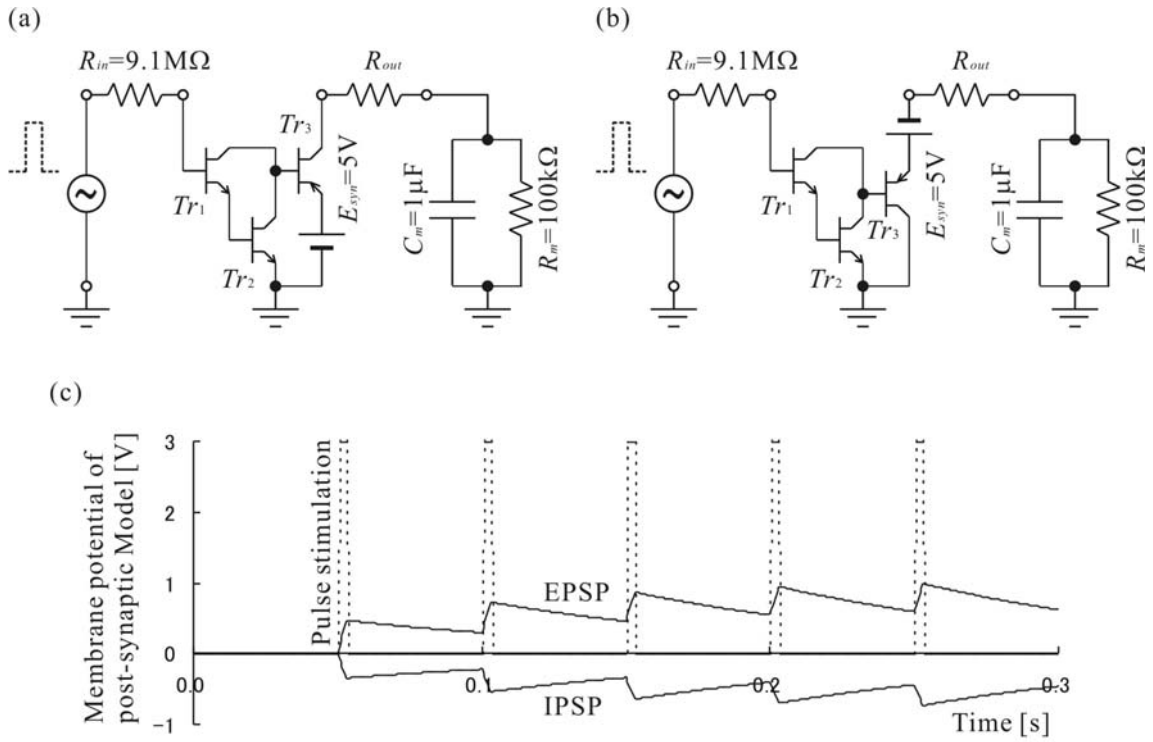


Fig. 5 (a) Excitatory synapse driven by a pre-synaptic pulse voltage and the post-synaptic simple R_m - C_m model (passive model). (b) Inhibitory synapse driven by a pre-synaptic pulse voltage and the post-synaptic simple R_m - C_m model (passive model). (c) Typical temporal waveforms of EPSP and IPSP ($R_{out} = 30\text{ k}\Omega$). The dotted lines represent the voltage pulse stimulation of the input.

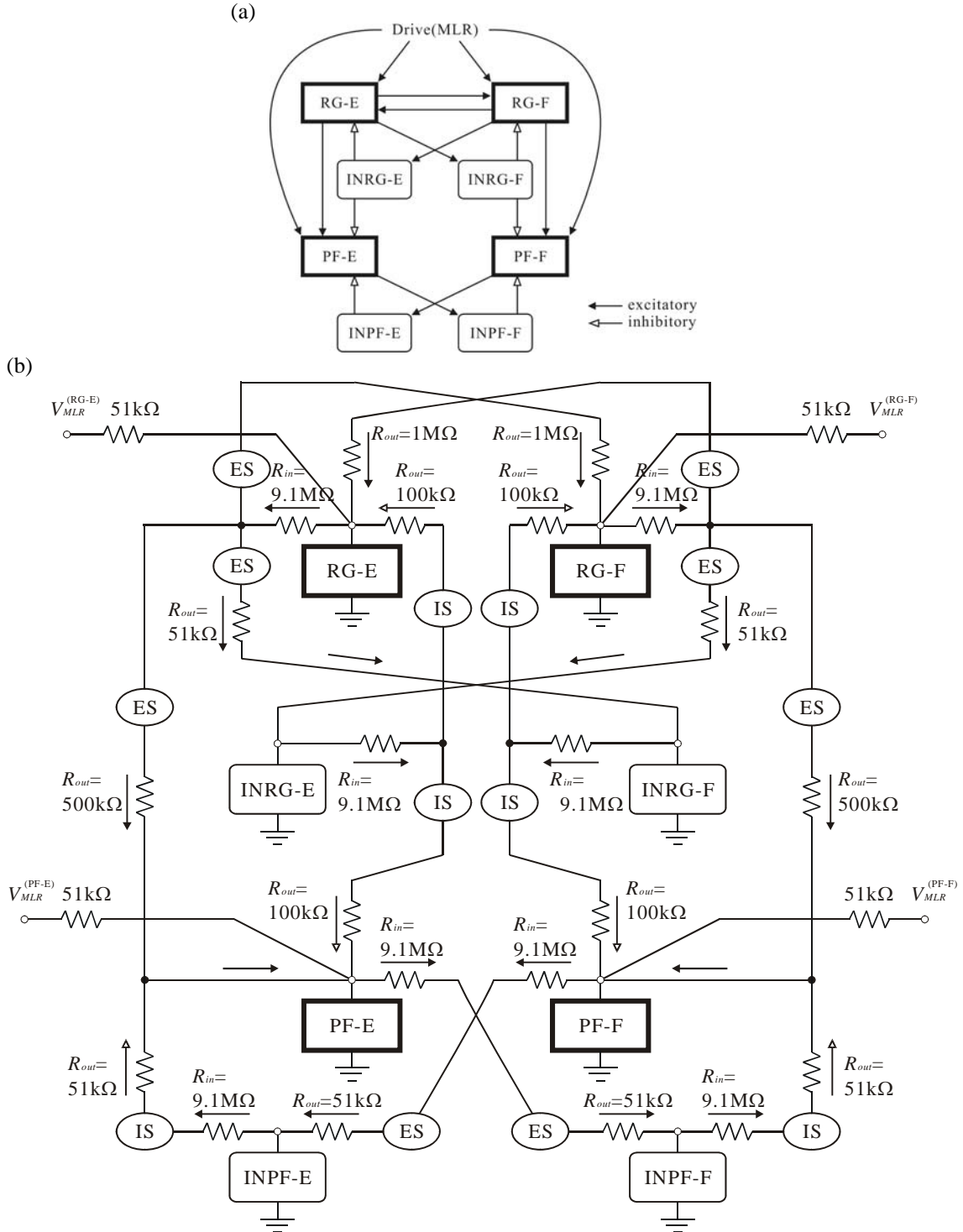


Fig. 6 (a) Schematic diagram of the two-level CPG. (b) Hardware configuration of the two-level CPG. “-E” and “-F” represent the extensor and flexor side, respectively. “RG”, “PF”, “IN”, “ES” and “IS” represent rhythm generator, pattern formation, interneuron, excitator and inhibitory synapses, respectively. Only RG was composed from the bursting model. Black and white arrows represent the excitatory and inhibitory flows of electrical information, respectively. $V_{MLR}^{(RG-E)}$, $V_{MLR}^{(RG-F)}$, $V_{MLR}^{(PF-E)}$ and $V_{MLR}^{(PF-F)}$ are external inputs (MLR) of RG-E, RG-F, PF-E and PF-F, respectively.

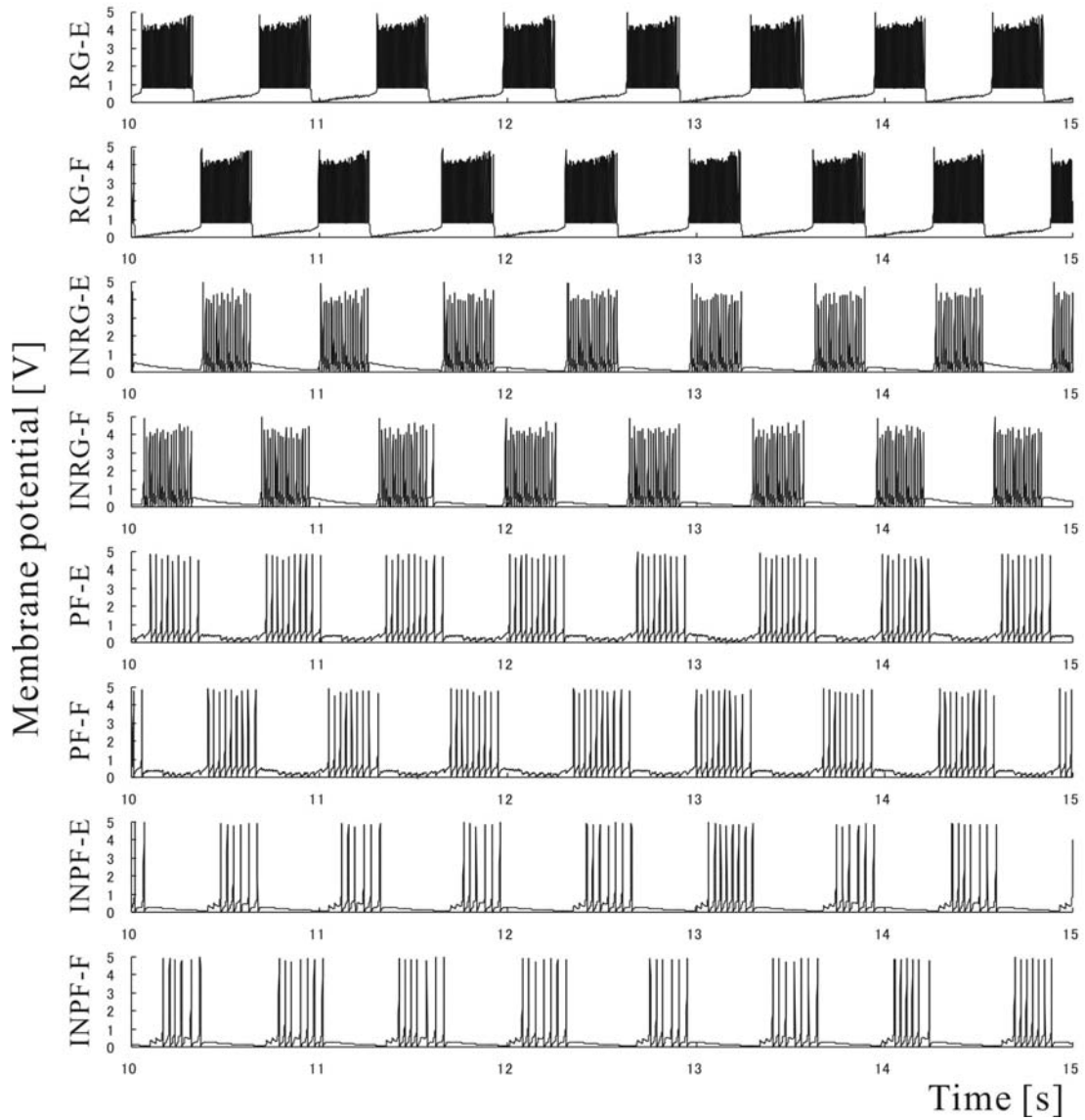


Fig. 7 Typical temporal waveforms of the membrane potentials from the hardware CPG model.

Externally injected constant voltage is 1.01V in RG-E and PF-E, and 1.0V in RG-F and PF-F.

Yoshinobu MAEDA

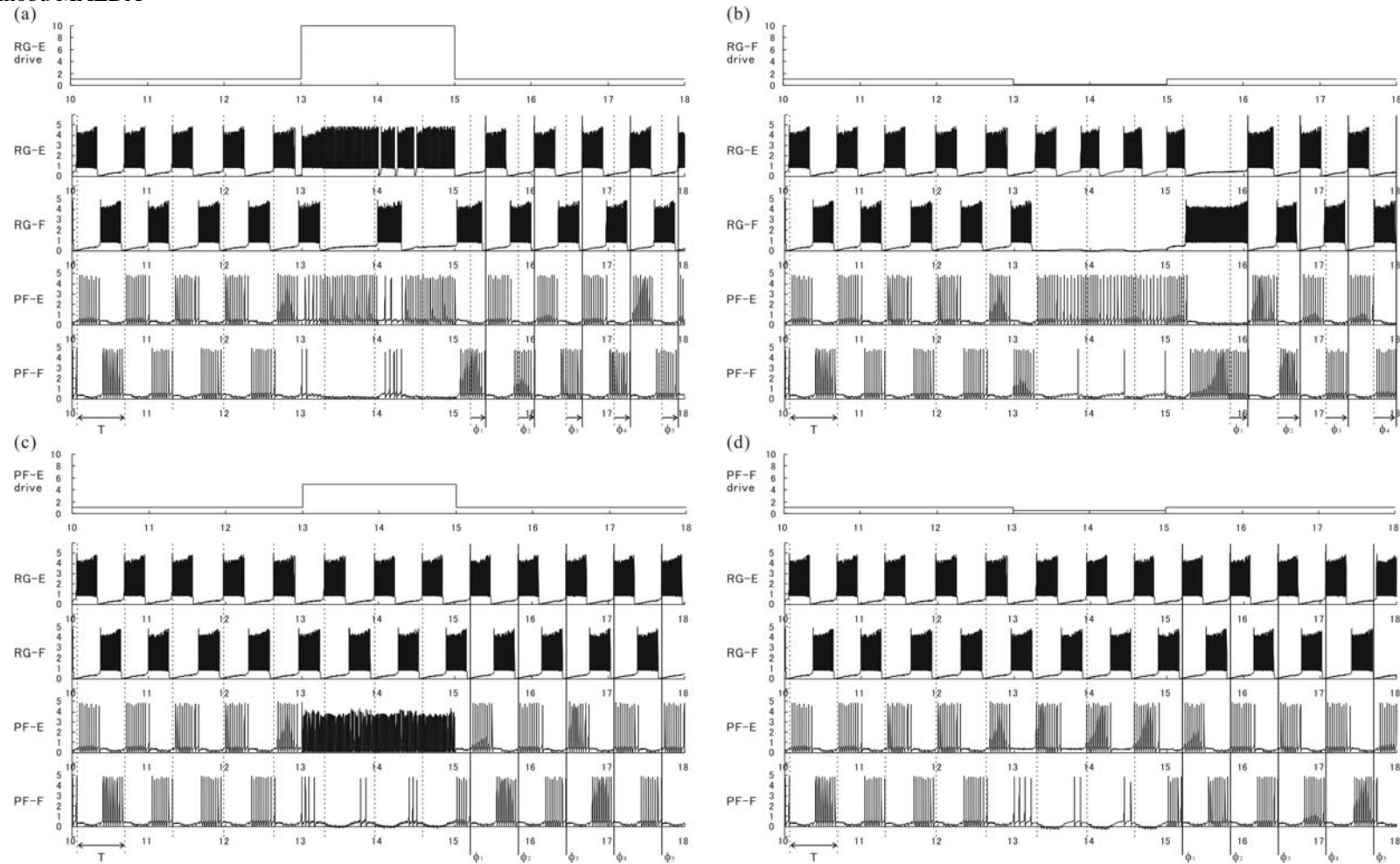


Fig. 8 Simulations of resetting deletions (phase shift) in (a) and (b), and non-resetting deletions (no phase shift) in (c) and (d) for the CPG model. RGs and PFs are originally driven by $V_{MLR}=1.01V$ and $=1V$, respectively. During 2 seconds from 13 to 15, the CPG model is additionally driven by the step-wise perturbation of (a) $V_{MLR}^{(RG-E)}=10V$, (b) $V_{MLR}^{(RG-F)}=0.1V$, (c) $V_{MLR}^{(PF-E)}=5V$, and (d) $V_{MLR}^{(PF-F)}=0.5V$.

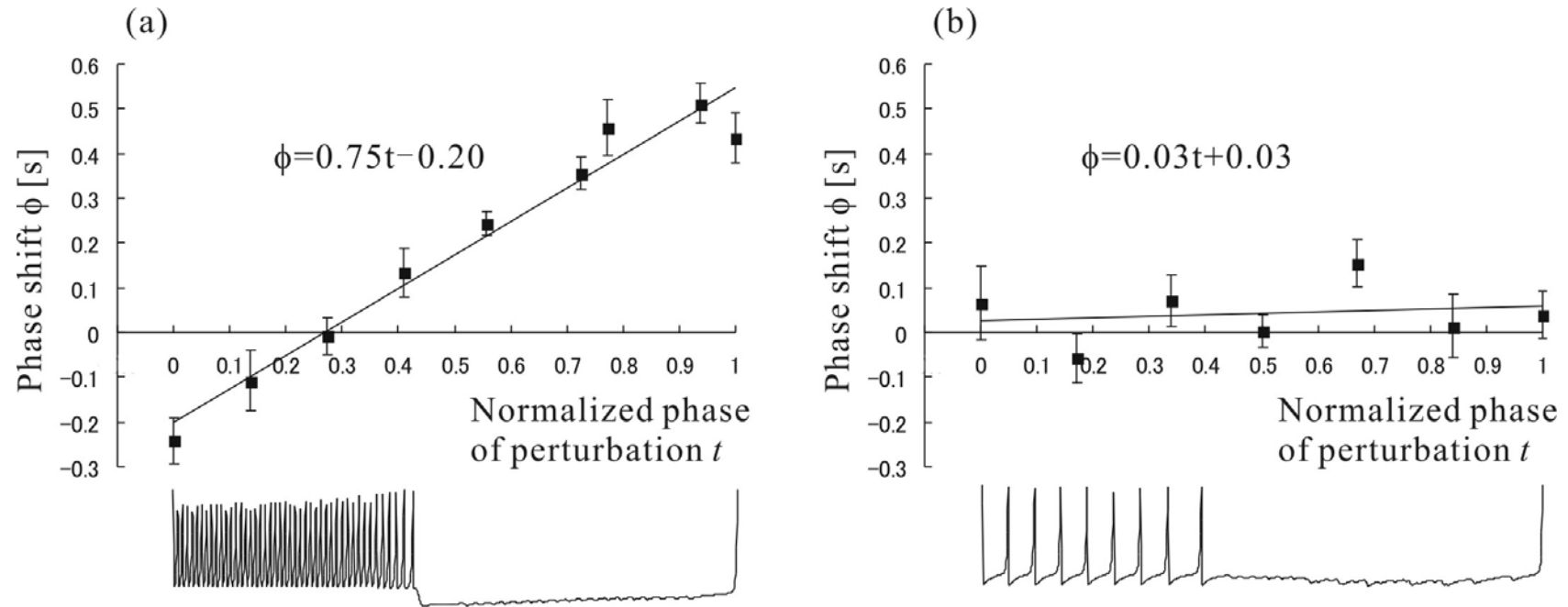


Fig. 9 Simulations of (a) resetting and (b) non-resetting deletions. Average phase shift ϕ vs normalized phase of perturbation t . Normalized phase corresponds to the temporal waveforms illustrated below. The active phase of bursting corresponds to the duration from 0.0 to 0.4 of the normalized phase.